Use of OTA System Performance Metrics in the Design & Optimization of CATRs for 5G Testing

S.F. Gregson [1, 2]
[1] Next Phase Measurements
11521 Monarch St
Garden Grove, CA, USA
stuart.gregson@qmul.ac.uk

C.G. Parini [2]
[2] School of Electronic Engineering and Computer Science
Queen Mary University of London
London, UK
c.g.parini@qmul.ac.uk

***Abstract*—Delivering on the promise of 5G measurements requires the adoption of new RF system technologies that encompass both the mobile user equipment and the active base station. Keeping pace with the impact of new wireless system test parameters such as: Data throughput, Error Vector Magnitude, Symbol Error Rate, and technologies such as mm-wave Massive MIMO, OFDM, and QAM presents significant challenges to antenna test community. For the most part, the market has attempted to react by adapting traditional test equipment to the wireless market however 5G testing presents an ever-greater challenge and demands the incorporation of simulation effects when designing and optimising an antenna test system, especially as these systems have increased in complexity with the adoption of the indirect far-field method and specifically the compact antenna test range (CATR). This paper discusses how 5G communication system parameters affect the design of the CATR and how newly developed simulation capabilities have been incorporated to optimize the CATR design for 5G test applications.**

I. Introduction

5G New Radio (5G NR) is a completely new air interface that is being developed for the next generation of mobile telecommunication systems. 5G NR makes several significant promises regarding improvements in the user's mobile experience including: delivering enhancements in performance, efficiency, scalability and flexibility of the radio access network (RAN). However, of these, perhaps the multi-Gbps increase in data capacity is the most significant [1]. Delivering on this promise requires the adoption of new technologies in the RF system that encompasses both the mobile user equipment and the active base station. Of these, the use of higher frequency, millimetre wave, bands and the widespread deployment of more complex, electrically larger, massive MIMO (Multiple Input Multiple Output) antenna architectures are possibly the most significant changes [1, 2]. The required ten to twenty-fold increased in absolute data throughput mandated by the 5G NR promise has, furthermore, resulted in the adoption of absolute data throughput becoming the primary Figure of Merit (FOM) used for the verification of network performance. The adoption of Over the Air (OTA) communication system performance parameters has resulted in two changes. Firstly, classical far-field antenna parameters have become far less significant than was previously the case with instead, focus largely shifting toward communication system level parameters such as far-field error vector magnitude (EVM), bit error rate (BER), signal-to-interference-plus-noise-ratio (SINR) and of course, absolute data throughput. Secondly, the increase in complexity and electrical size of the massive–MIMO antenna system when combined with the near exclusive use of orthogonal frequency-division multiplexing (OFDM) family of waveforms – predicating the use of quadrature amplitude modulation (QAM) schemes – has resulted in the indirect far-field (IFF) method becoming the only technique that has been approved for OTA testing of all three antenna classes by the 3rd Generation Partnership Project (3GPP) [3].

The renewed interest in the IFF method, and specifically the compact antenna test range (CATR) [4, 5], stems from the inherent advantage that it provides a way to obtain real-time, broadband, far-field performance at a very much reduced, fixed distance, *i.e.* a range-length that is independent of frequency, *cf.* equation (1) below. This is of great importance for 5G applications where testing the higher-frequency, larger electrical aperture sizes required by active mm-wave massive-MIMO antennas results in path-losses and far-field distances that are very much larger than those which were previously encountered when testing equipment for earlier generations of RAN at sub-6 GHz frequencies and which cannot otherwise be implemented economically indoors.

TABLE I. Illustration of Range Length and Spherical Path Loss for Various 5G Measurements.

Frequency (GHz)	Size (cm)	Far-Field Distance (m)	Attenuation (dB)
26	10	1.7	66
	15	3.9	73
	20	6.9	78
39	10	2.6	73
	15	5.9	80
	20	10.4	85

This situation is illustrated in Table I where it can be seen that only the electrically smallest test articles can be accommodated within a standard, typical 3 m long, OTA test chamber. Here, the range length is computed from the Rayleigh far-field formula and the loss from the Friis

transmission formula, *i.e.* respectively, where c denotes the speed of light,

$$R = 2D^2 f / c \tag{1}$$

$$\text{Path Loss Factor}_{dB} = -20\log_{10}\left(\frac{c}{4\pi R f}\right) \tag{2}$$

The pseudo plane-wave generated by the CATR upon reflection of the feed pattern by a parabolic reflector which has the effect of projecting an image of the feed to infinity. This process provides an amplitude and phase taper which is generally far less than that provided by a typical direct far-field range. This is by virtue of the fact that at the typical far-field distance the phase curvature across the AUT is 22.5˚ (*i.e.* $\pi/8$ rad) and even at twice this distance the variation is only reduced to 11.25˚ which even here is slightly larger than the peak-to-peak phase ripple permitted by conventional CATR QZ performance specifications [4]. Thus, the CATR based IFF method provides a convenient, spatially efficient measurement technique for all test articles providing only that they fit within the CATR QZ. Figure 1 illustrates the operation of a CATR by showing the pseudo plane wave, *i.e.* a transverse electric and magnetic (TEM) wave, produced by the CATR coupling into the aperture fields of the AUT. By measuring this coupled power as a function of angular orientation of the AUT we may tabulate the conventional measured far-field antenna pattern.

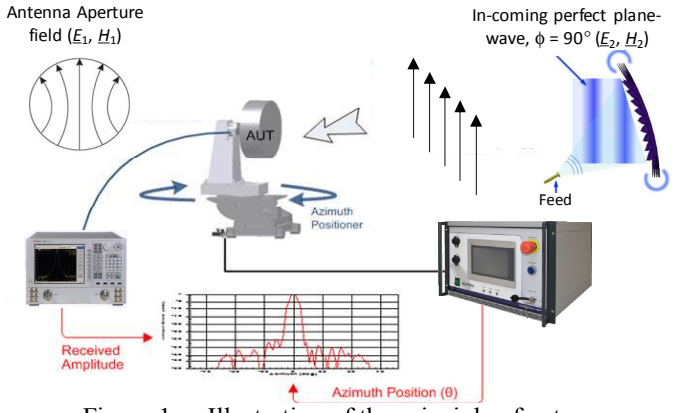

Figure 1. Illustration of the principle of antenna measurement in a CATR.

This process of coupling can be expressed mathematically by equation (3) which is a statement of the power coupling formula that can be derived from a reciprocity relation [4].

$$P = \left| \left\{ \frac{1}{2} \int_{S_2} \left(\underline{E}_1 \times \underline{H}_2 - \underline{E}_2 \times \underline{H}_1 \right) \cdot \hat{\underline{n}} \, ds \right\} \right|^2 \tag{3}$$

Thus, we see that the quality of our measurement depends to a large extent on how well $\underline{E}_2$ & $\underline{H}_2$ approximate a perfect TEM wave across the AUT. This in turn depends on the feed pattern, reflector size, reflector edge treatment/diffraction & reflector surface profile, feed & reflector alignment, location of QZ, *etc*. Thus, to be able to optimise our CATR, we need to be able to predict the Fresnel diffraction pattern, *i.e.* the CATR QZ. Although CATR modelling is a well-established, mature discipline capable of determining the quiet-zone (QZ) [4] and measurement uncertainties for a range of typical antenna parameters for a known antenna under test (AUT) / CATR combination [4], it is only very recently that it has become possible to equate this to OTA communication system-level properties such as EVM, BER, *etc.* [5, 6].

In this paper we present the results of recent work that has extended our previously published simulation techniques [5, 6, 7, 8] to include these communication system performance metrics and have then examined their use in the design and optimization of a 5G test system that is intended for 5G Massive MIMO OTA testing applications. Example results are presented and discussed. The next section presents an introduction to the novel modelling technique.

II. Overview of OTA Measurement Simulation and Assessment Technique

Orthogonal Frequency-Division Multiplexing (OFDM) is a very flexible and efficient modulation technique that is at the heart of all major wireless and wired standards used today including 5G [3]. Examples of standards that use OFDM include: 4G, LTE, WiMAX, Video Broadcast, ADSL, 5G, *etc*. OFDM separates the channel bandwidth into multiple narrow-band subcarriers which are used to transmit the information. Here, a single data stream is split across several separate narrowband channels each at different frequencies. The original data stream of bits is transmitted in parallel but at lower speed in each sub-stream when compared to the original. Thus, for us to simulate the behaviour of the communications system we must compute the S_{21} transmission coefficient for the CATR and AUT combination at *each* of these frequencies. This results in a computationally intensive problem as a typically a 5G signal may operate across a 400 MHz bandwidth resulting in the need for *circa* 201 carriers. Thus, we may use the methodology presented in the preceding section to compute the channel, *i.e.* S_{21} transmission coefficient between the range and the AUT as this corresponds to a single point in the far-field antenna pattern, for a fixed orientation between AUT and range. However, what we have presented up to now is essentially a Frequency Domain modelling technique, [4]. Thus, we would need to repeat this simulation across a *range* of frequencies, *i.e.* channels. And, although the feed pattern remains fairly stable across the comparatively narrow 400 MHz bandwidth required by 5G applications, resulting in the amplitude taper also remaining fairly stable with frequency; the amplitude and phase ripple in the CATR QZ will vary with frequency as these are governed by edge diffraction from an electrically large structure which are frequency dependent. Furthermore, the antenna Gain can be expected to vary with frequency (typically increasing for the case of an aperture antenna) with the location of the side-lobes also changing with frequency which can become more pronounced as the beam may be electronically steered. Thus, we can expect the behaviour of the channel to vary over the frequency range used by a 5G communications system. Although we require the computationally intensive evaluation of one complete CATR / AUT simulation per frequency, this is essentially parallel in nature meaning that actual processing times can be made practical providing that these simulations are deployed taking advantage of the parallel nature of the problem.

Thus, the first step in the simulation is to harness the methodology set out within the preceding section, and detailed within the open literature [4], to compute the "Measured" far-field pattern of AUT for a known AUT – CATR combination at, in this example, 26 GHz. Figure 2 and 3 present the results of this simulation where we have plotted the ideal far-field pattern of a mm-wave Back-Haul massive MIMO antenna, red trace, typical of that used in 5G applications and compared this against the CATR pseudo plane wave AUT measurement, blue trace. Here, the CATR has a QZ of 0.46 m diameter and is very typical of the type of test system conceived for 5G test and measurement applications. Additionally, as a measure of adjacency we have plotted the equivalent multi-path level (EMPL) as a measure of agreement [7]. Here, some differences are evident and are as result of the small imperfections in the pseudo plane wave formed by the CATR.

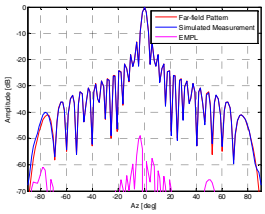

Figure 2. Comparison of ideal and "measured" patterns of 5G MIMO antenna amplitude.

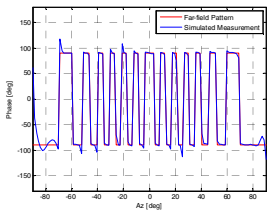

Figure 3. Comparison of ideal and "measured" patterns of 5G MIMO antenna phase.

These simulations were then repeated at each required frequency across the 400 MHz 5G band. For a given AUT / CATR orientation, *i.e.* pattern angle, the complex S_{21} transmission coefficient was extracted. This can be seen presented in Figure 4 below where the S_{21} amplitude and phase have been plotted as a function of frequency for a single AUT / CATR orientation.

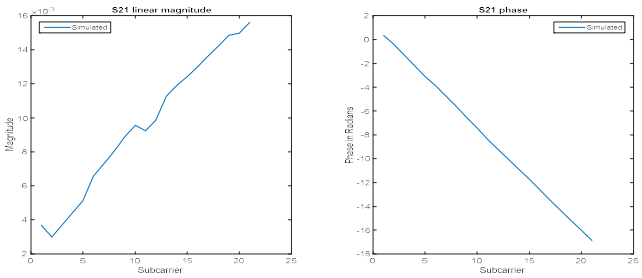

Figure 4. Simulated Amplitude and phase S_{21} results for a 5G Massive MIMO antenna working at 26 GHz across a 400 MHz band.

For the purposes of the OTA communications system simulation a standard image was chosen to be the information to transmit [5, 6]. An image was selected as the eye is very sensitive at discerning errors. Here, a 512 x 512 RGB (red green blue) image with 8 bits per pixel was used. The data was encoded using 256 QAM modulation with a 16 x 16 constellation using 8 bits per pixel. Here, the number of constellation points within the diagram determines the size of the "alphabet" of symbols that can be transmitted by each sample which determines the number of bits transmitted per sample with 256 being a commonly used order. The image data was then mapped byte by byte onto the symbols so that each symbol error produces an error within one colour channel of one pixel. The transmission of the data was simulated by assuming that for the OFDM case, each frequency in the input being treated as a separate subcarrier. Thus, the transmitted signal was scaled by S_{21} which represents the channel, *i.e.* the CATR/AUT transmission line. The received signal then must be equalised before we may recover the transmitted data. Once we have decoded the transmitted data, we can calculate several typical communication system level figures of merit by comparing the received data set against the original unperturbed data.

The need for equalisation derives from noting that attenuation of the transmitted signal reduces the size of the QAM constellation diagram whereas the phase delay rotates the constellation diagram. For the received signal to be correctly decoded, the received signal must be equalised to recover the transmitted information and be equalised in a way that is representative with what would be experienced in practice. Thus, quality of the equalisation used directly effects the result. By way of a further illustration, Figure 5 presents the measurement of an equalised measured received signal. Here, the amplitude is correctly normalised across the frequency band.

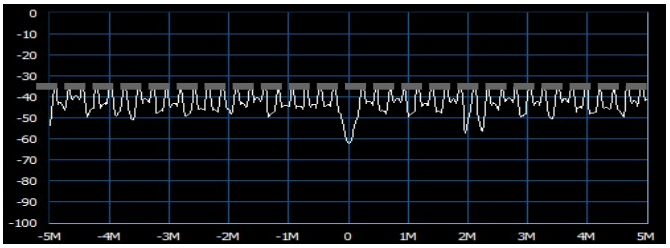

Figure 5. Example of a real measured signal (dBm). Each peak represents a channel in the signal. The dotted line illustrates the need for uniformity in the signal.

For the purposes of this study, a similar technique was used for the equalisation as is found in many practical applications. This involved periodically transmitting a known symbol. This information was then used to correct the nearby symbols by means of a complex linear estimate, *i.e.* providing both amplitude and phase correction.

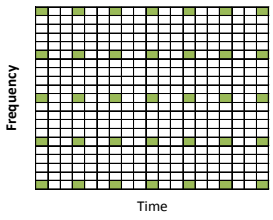

Figure 6. Frequency time diagram showing green reference symbols.

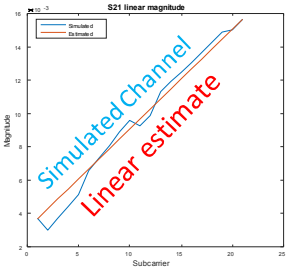

Figure 7. Ilustration of channel equalisation.

This is illustrated in Figure 6 which presents a frequency time diagram with the reference symbols being denoted in green with Figure 7 showing the linear equalisation plotted together with the simulated channel. Although this is a

comparatively simple form of complex channel equalisation, it was verified experimentally and found to yield results that were in good agreement with what one sees in a practical implementation. Clearly then, this complex linear channel equalisation procedure can be expressed mathematically as,

$$\text{Equalised Symbols} = \text{Symbols} \times \frac{\text{Channel}}{\text{Channel Estimate}} \tag{4}$$

Once equalised, the received signal can be decoded, and the resulting data may be assessed to determine its quality by, for example, inspection as a standard image was used as the underlying dataset. As no communications channel is perfect, we need a measure of quality. Error Vector Magnitude (EVM) is a measure of the modulator or demodulator performance of an impaired signal [2, 3, 5]. Its appeal stems from recognising that from this RF based quantity, we can calculate other figures of merit, *e.g.* SINR [5]. Here, EVM can be computed from the equalised received signal using,

$$EVM_{RMS} = 100 \sqrt{\frac{\frac{1}{N}\sum_{k=1}^{N} e_k}{\frac{1}{N}\sum_{k=1}^{N}\left(I_k^2 + Q_k^2\right)}} \tag{5}$$

Here, the RMS value of the EVM is expressed in terms of a percentage, N denotes the number of symbols, e_k is the difference between ideal and actual received symbols and I_k and Q_k are in in-phase and quadrature components of the received QAM signal. Several different normalisation schemes can be used when calculating EVM however here we normalised to the signal, normalising to average power or peak power are both valid alternatives. Thus, we may assess the impact of a CATR on our communications systems OTA measurements. We may calculate the EVM which can be interpreted as an RF measure of performance. Alternatively, we may compare the original dataset with the recovered dataset and calculate the bit error rate, which we may also express as a percentage and can be interpreted as a digital measure of performance. This is useful as BER can be used to calculate absolute data throughput as this is approximately equal to $R(1 - \text{BER}/100)$ where R is the data rate. In the event of the occurrence of errors, then we need to resend the data and throughput drops further. More complete formulae are available for computing the data throughput, *cf.* [3], however the basic idea remains the same. Lastly, we may assess the success from a cognitive perspective by using, for example, the Image Structural Similarity Index (normalised measure) for measuring image quality [9]. This is an objective, quantitative, holistic way of "looking" at the recovered image. To illustrate the use of these metrics, for the case of perfect transmission, Error Vector Magnitude (RMS) = 0.0 %, Symbol Error Rate = 0.0 % and the Structural Similarity Index = 1.0. For the case of zero data transmission, these metrics respectively will have the values 100%, 100% and 0.0.

This section, together with the previous one, has presented the novel OTA communications system performance prediction model together with several ways in which the quality of the transmission can be assessed. The following section presents results of several simulations that illustrate the utility of the technique.

III. RESULTS

The representative 5G CATR / AUT combination considered in Section II above was utilised to model the transmission of a reference 512 x 512 RGB (red green blue) image using 8 bits per pixel. Here the "Lenna" standard test image was used [10]. Use of this 512 x 512 image is "overlooked" and by implication permitted by Playboy [10]. Alexander Sawchuk *et al* scanned the image and cropped it specifically for distribution for use by image compression researchers and hold no copyright on the image. The data was encoded using QAM modulation with an order of 256 and transmitted across a 400 MHz bandwidth at 26 GHz. Linear equalisation was used, and results obtained for the case where the AUT was rotated to a number of different orientations allowing the simulation of an EVM cut, where EVM is presented as a percentage and plotted as a function of angular orientation [11]. Of those, and due to the constraints of space, two cases have been chosen to be presented here as they demonstrate firstly near error free transmission at 10˚ and then severely degraded date transmission at 30˚. Figure 8 below presents the results of the OTA communications simulation for the case where the AUT was rotated by 10˚. The left-hand image is a 16 by 16 constellation diagram comparing transmitted (blue) and equalised received (red) constellation points. Here, it is clear that the transmitted and received signals are in close agreement (as comparatively little red is visible). The data is decoded, and the recovered image plotted, centre, with a close-up image presented at the right-hand side of the figure. From inspection the image appears clean with no visible defects or digital transmission artefacts.

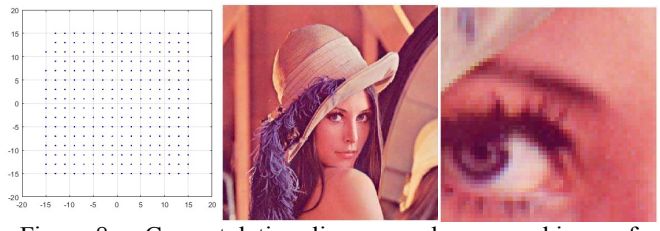

Figure 8. Conmstalation diagram and recovered image for the case of the massive MIMO antenna rotated to 10˚.

This observation is further corroborated by the EVM which was found to be 0.1%, the symbol error rate was 0%, as each point in the constellation diagram fell within the local of the ideal point. This immunity to noise is the fundamental advantage of digital communication systems and is the reason which the received data set, *i.e.* the image, is error free with a structural similarity measure of unity. The reason for this success is that the linear equalisation process accurately represented the behaviour of the channel. In the event that this is not the case, the communications system will struggle to recover the transmitted data. This situation is highlighted by the 30˚ case now considered. Figure 9 contains a similar figure only here the AUT has been rotated so that the transmission is through the wide-out sidelobe region. As before, left-hand image is a 16 by 16 constellation diagram comparing transmitted (blue) and equalised received (red) diagrams. Here, the transmitted and received signals are in significant

disagreement as a great deal of red is visible indicating the displacement of the recovered constellation points from their ideal rectangular lattice. There is therefore a spreading of the spots within the constellation which decreases the separation between the adjacent states which makes it difficult for the receiver to decode the signal correctly. The decoded image is plotted centre, with a close-up image presented to the right-hand side of the figure. From inspection the image appears degraded with visible defects and digital transmission artefacts.

Figure 9. Conmstalation diagram and recovered image for the case of the massive MIMO antenna rotated to 30˚.

This observation is corroborated by the EVM which was found to be 62.5%, the symbol error rate was 86.8%, with a structural similarity measure of 0.3. The primary reason for this is that the linear equalisation process is unable to accurately adjust the neighbouring/nearby symbols as in the region of a wide-out sidelobe the pattern changes rapidly as a function of frequency. This can be seen in Figure 10 where the amplitude and phase channel information are plotted together with the linear equalisation function.

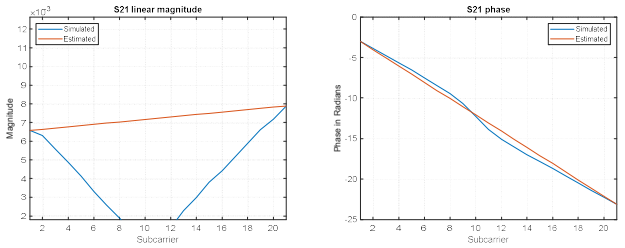

Figure 10. Conmstalation diagram and recovered image for the case of the massive MIMO antenna rotated to 30˚.

Here, the channel information is denoted by the blue trace with the red trace representing the equalisation. The quality of the recovered data would be significantly improved if reference symbols were transmitted more frequently or if a more sophisticated form of equalisation were chosen. The best form of equalisation is the form that is most closely represents that which is used by the actual hardware and that will vary on a case by case basis.

IV. Summary & Conclusion

This paper has presented a novel technique for simulating the effect that a known CATR would have on a conventional OTA communication systems measurement and comprises a more detailed treatment of the work previously presented in the open literature [5, 6]. The CATR simulation allows us to predict the "measured" far-field for a known AUT / CATR combination. This is used to compute the effect on EVM that a given CATR would have if used to measure a known 5G device under test (DUT) thereby allowing the designer to examine the effect that some particular attribute of the range, *e.g.* reflector size, edge treatment *etc.*, may have on EVM *etc*. The simulation has been verified experimentally and allows us to determine which parameters in a CATR are most important for a given 5G test application. Furthermore, and using this methodology, it is possible to convert between conventional uncertainties and EVM, BER *etc*. and use this information to optimise the design of a CATR, or any test system, that is intended for communications (5G) testing applications. In principle, it is possible, with full knowledge of the channel to successfully equalise almost any signal. Through the modelling we, in principle, know the exact behaviour of the channel. However, in practice the equalisation process applied within the simulation should represent that which is employed by the actual hardware under consideration so that reliable results are obtained avoiding the risk of overly optimistic or pessimistic values for the EVM, data throughput *etc*. Finally, the future work is to include repeating the assessment using more representative equalisation techniques, assessing the impact of imperfections on the CATR QZ on the measurement of 5G parameters and evaluating the effect of CATR QZ on the calibration of mm-wave massive MIMO antennas.

Acknowledgement

The authors gratefully acknowledge the help and support of Huawei Technologies and the UK National Physical Laboratory.

References

[1] Wonil Roh, "5G Mobile Communications for 2020 and Beyond - Vision and Key Enabling Technologies," IEEE WCNC 2014 Keynote, Apr. 2014.

[2] Z. Pi and F. Khan, "An introduction to millimeter-wave mobile broadband systems," IEEE Commun. Mag., vol. 49, no. 6, pp. 101–107, Jun. 2011.

[3] *NR; Study on test methods, 3GPP TR 38.810: Release 16*, Table 5.3-2, Page 29, March 2019.

[4] C.G. Parini, R. Dubrovka, S.F. Gregson, "CATR Quiet Zone Modelling and the Prediction of "Measured" Radiation Pattern Errors: Comparison using a Variety of Electromagnetic Simulation Methods" AMTA October 2015.

[5] S.F. Gregson, C.G. Parini, "Compact Antenna Test Ranges: The Use of Simulation and Post-Processing Techniques in Support of 5G OTA Testing" EuCAP 2019 Invited Plenary Presentation, April 2019.

[6] S.F. Gregson, C.G. Parini, D.A. Humphreys, D. Cheadle "Simulation of OTA System Performance Parameters in a mm-Wave CATR for 5G Testing" EuCAP 2019 Huawei Scientific Workshop, Invited Presentation, April 2019.

[7] C.G. Parini, S.F. Gregson, J. McCormick, D. Janse van Rensburg "Theory and Practice of Modern Antenna Range Measurements", IET Press, 2014, ISBN 978-1-84919-560-7.

[8] S.F. Gregson, C.G. Parini, "Examination of the Effect of Common CATR Quiet Zone Specifications on Antenna Pattern Measurement Uncertainties", Loughborough Antennas and Propagation Conference, November 2017.

[9] Z. Wang, A. C. Bovik, H. R. Sheikh, and E. P. Simoncelli, "Image Quality Assessment: From Error Visibility to Structural Similarity," IEEE Transactions on Image Processing, Volume 13, Issue 4, pp. 600-612, 2004.

[10] Lenna, Wikipedia, https://en.wikipedia.org/wiki/Lenna, last accessed 18 July 2019, last edited on 17 June 2019.

[11] 3GPP TSG-RAN WG4 Meeting #81, R4-1609526.